



2nd Advanced Optical Metrology Compendium

Advanced Optical Metrology

Geoscience | Corrosion | Particles | Additive Manufacturing: Metallurgy, Cut Analysis & Porosity



EVIDENT
OLYMPUS

WILEY

The latest eBook from **Advanced Optical Metrology**.
Download for free.

This compendium includes a collection of optical metrology papers, a repository of teaching materials, and instructions on how to publish scientific achievements.

With the aim of improving communication between fundamental research and industrial applications in the field of optical metrology we have collected and organized existing information and made it more accessible and useful for researchers and practitioners.

EVIDENT
OLYMPUS

WILEY

Extreme Specific Stiffness Through Interactive Cellular Networks in Bi-Level Micro-Topology Architected Metamaterials

Diptiman Kundu, Sushanta Ghuku, Susmita Naskar,* and Tanmoy Mukhopadhyay*

Architected lattice materials, realized through artificial micro-structuring, have drawn tremendous attention lately due to their enhanced mechanical performances in multifunctional applications. However, the research area on the design of artificial microstructures for the modulation of mechanical properties is increasingly becoming saturated due to extensive investigations considering different possibilities of lattice geometry and beam-like network design. Thus, there exists a strong rationale for innovative design at a more elementary level. It can enhance and grow the microstructural space laterally for exploiting the potential of geometries and patterns in multiple length scales, and the mutual interactions thereof. A bi-level design is proposed, where besides having the architected cellular networks at an upper scale, the constituting beam-like members at a lower scale are further topology-engineered for most optimum material utilization. The coupled interaction of beam-level and lattice-level architectures can enhance the specific elastic properties to an extreme extent (up to ≈ 25 and 20 times, depending on normal and shear modes, respectively), leading to ultra-lightweight multifunctional materials for critical applications under static and dynamic environments.

mechanical properties and multifunctionality. In many technologically demanding applications like aerospace structures, one of the key requirements is extreme minimization of weight while maintaining the other mechanical properties at an adequate level under complex loading conditions. The performance of these lightweight structures is mainly dependent upon the topological configuration, arrangement of unit cells, and relative density. This article aims to propose a radical measure of bi-level topology optimization for achieving an unprecedented enhancement of specific stiffness in such lattice materials.

The unit cell-based approach to analyzing periodic lattices has been widely adopted in the literature.^[8–12] These materials have tunable mechanical properties as the global-level physical behavior is not only dependent upon the intrinsic material, but the microstructural geometry of the periodic units also. The macro-scale lattice properties like Young's moduli,^[13,14]

Poisson's ratio,^[15] and shear moduli^[16] are largely dependent upon the geometric configurations of the periodic unit cells.^[17,18]

In most cases, the unit cells can be imagined as a network of beam-like solid elements. Thus, in turn, the global physical properties of a lattice material depend on the deformation physics of the beam-like elements and the microstructural topology of lattices, describing how the beams are connected to form the unit cell. These lattice materials have an open cell structure and have a relatively lower density providing enhanced mechanical properties^[19,20] compared to conventional materials. Intense research has been performed recently on multi-physical and multi-material property modulation,^[21–25] nanoscale multifunctional properties,^[26–28] far-field actuation dependent local shape and stiffness modulation^[29–32] and auxetic metamaterials.^[33,34] Tremendous progress in 3D printing and other manufacturing technologies^[35–37] over the past decade has boosted the physical realization of complex metamaterial designs and experimental investigation for such lattices.


The concept of topological periodic network design for lattice microstructures has become rather saturated lately due to extensive investigations over the past decade.^[8,38,39] Thus, there exists a strong rationale for more innovative design at the elementary level^[40–43] that can bring about a radical expansion in the available design space to have significant improvement by pushing

1. Introduction

Engineering structures featuring lattice materials^[1–7] have tremendous potential applications in the field of defense, aerospace, biomedical, mechanical, and civil engineering due to an unprecedented level of tolerability, the capability of achieving extreme

D. Kundu, S. Ghuku, T. Mukhopadhyay
Department of Aerospace Engineering
Indian Institute of Technology Kanpur
Kanpur 208016, India
E-mail: tanmoy@iitk.ac.in

S. Naskar
Faculty of Engineering and Physical Sciences
University of Southampton
SO17 1BJ Southampton, UK
E-mail: S.Naskar@soton.ac.uk

 The ORCID identification number(s) for the author(s) of this article can be found under <https://doi.org/10.1002/adem.202201407>.

© 2022 The Authors. Advanced Engineering Materials published by Wiley-VCH GmbH. This is an open access article under the terms of the Creative Commons Attribution License, which permits use, distribution and reproduction in any medium, provided the original work is properly cited.

DOI: 10.1002/adem.202201407

the boundaries of mechanical characteristics such as specific stiffness under normal and shear modes. In this article, we propose to exploit more elementary-level topology optimized beams in place of the conventional solid cell walls besides having unit cell level architecture. The expanded microstructural design space would lead to a unique interaction between the beam level and unit cell level topological architecture for the most optimum utilization of material.^[44] This would be the first attempt to couple the concept of topology optimization with microstructural periodic lattice network design.

The research on topology optimization of structural elements^[45–48] has drawn increasing attention from the engineering and scientific community in the past few years to use natural resources optimally. Topology optimization has expanded itself in areas of continuum structures^[49–51] to nonlinear structural applications.^[52] The field has developed rapidly with many new contributions to theory, computational methods, and their applications in aerospace structures.^[53] Topology optimization of continuum and discrete solid structures involves the determination of features such as the number, location, and

shape of voids along with connectivity of the domain that builds up the structure. The method includes both sizing and shape optimization. Sizing optimization focuses on optimal thickness distribution using minimization or maximization of any quantitative element like stress or deflection such that the constraints and equilibrium conditions are satisfied at the same time. As the name suggests, shape optimization deals with removing material from non-vulnerable places resulting in differently shaped voids. The density-based approach^[54–56] used in topology optimization distributes the material over the domain such that the raster representation of the domain constitutes elements either with the unit or null density. Finally, we get a lightweight structure with efficient use of the intrinsic material. The overarching objective of this article is to infuse the exciting capabilities of topology optimization for minimizing material utilization in novel microstructural design and further expand the scope of mechanical metamaterials following a seamless bottom-up bi-level computational framework (refer to **Figure 1**).

We would first analyze the beams that constitute a unit cell of the lattice and contribute to the lattice-level mechanical behavior

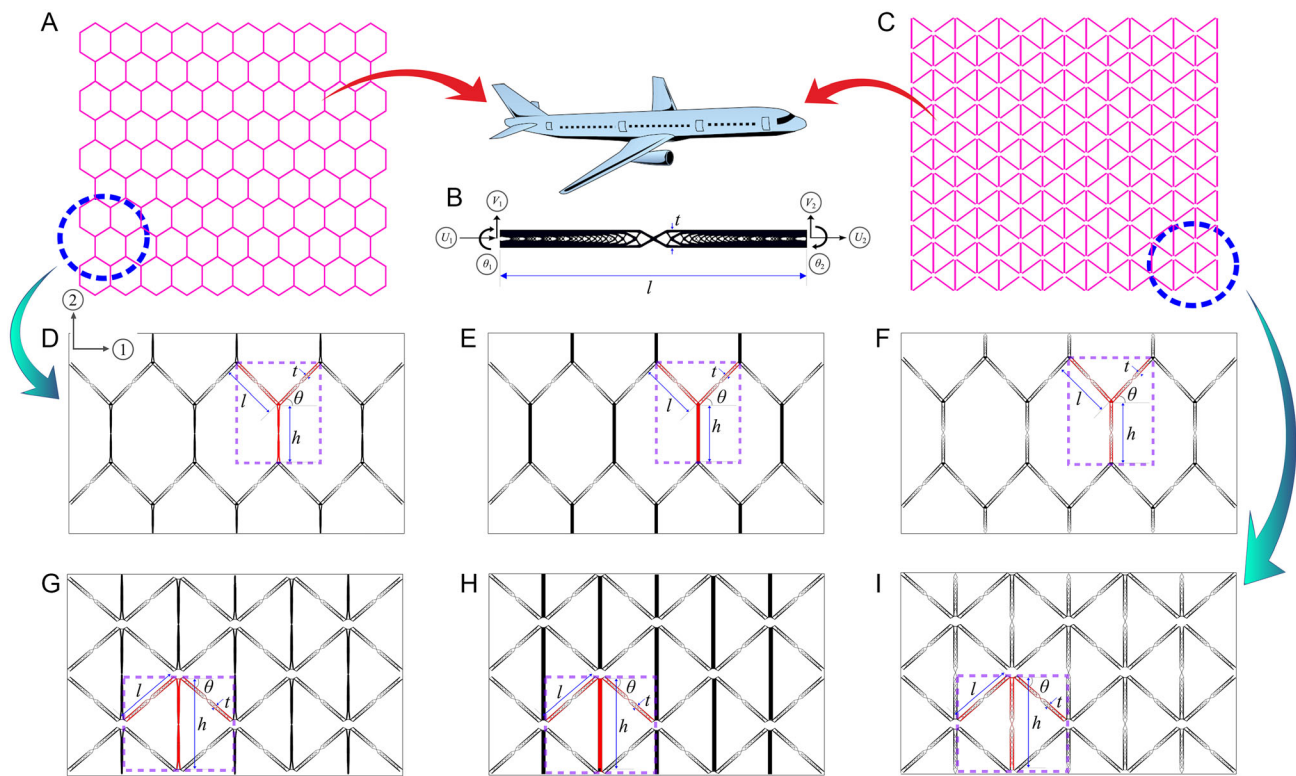


Figure 1. Bi-level design of topology-optimized lattice materials. A,C) General non-auxetic and auxetic hexagonal lattices. Such microstructures can be used for novel material development using unit cell-level geometries. These multifunctional materials can find applications in technologically demanding structural systems such as aerospace structures. B) A topology-optimized beam element with any arbitrary solid volume fraction representing the constituent member of the lattice. Proper representation of the degree of freedom (DOF) is shown at the two end nodes. U_1 and U_2 show the local DOF along the horizontal direction, V_1 and V_2 show the local DOF along the vertical direction and θ_1 and θ_2 show the rotational DOF. Note that the adoption of topology-optimized beams allows the proposed bi-level design at the unit cell level and at the beam level. D,G) Non-auxetic and auxetic lattices with topology optimization applied on both vertical and inclined members. These lattices can be typically used against normal loading along directions 1 and 2. E,H) Non-auxetic and auxetic lattices with topology optimization applied only on inclined members. These lattices can be typically used against normal loading along directions 1 and 2. F,I) Non-auxetic and auxetic lattices with topology optimization applied on both vertical and inclined members. These lattices can be typically used against the shear mode of in-plane loading. The nature of topology optimization in the slant and vertical members subjected to bending and axial deformations depends on the normal and shear stresses applied remotely.

depending on the applied lattice-level far-field (i.e., remote) stresses and beam orientation within the unit cell. At this stage, a computational framework of topology optimization will be exploited to minimize the material utilization of the beams considering appropriate boundary conditions and the normal or shear mode of far-field stresses.^[56] The axial and transverse deformation of such topology-optimized beams would be seamlessly integrated with the unit-cell level lattice architecture subsequently to obtain the effective elastic properties of the periodic lattices. Typical configurations of the proposed novel lattices with optimized cell walls under different modes of applied far-field stress are shown in Figure 1D–I. It may be noted in this context that the proposed lattices show different beam-level optimized topologies depending on the stress resultants and the boundary conditions, which in turn depend on the unit cell geometry and normal or shear modes of applied far-field stresses. While in this article we would concentrate on hexagonal lattices with auxetic and non-auxetic configurations (as shown in Figure 1), the bi-level bottom-up framework would be applicable for any other forms of bending and stretching dominated lattices in the 2D and 3D spaces. Our focus here is on the full spectrum of effective in-plane elastic moduli such as (longitudinal and transverse) Young's modulus, shear modulus, and two Poisson's ratios, which can capture the entire constitutive matrix for 2D materials^[57] to demonstrate the enhancement of specific stiffness of the proposed lattice metamaterial under the application of far-field normal and shear stresses. The basic underlying mechanics of the proposed bi-level micro-topology architected lattice materials being scale-independent, this novel class of materials can be adopted in a range of milli-, micro-, and nanometer-level engineering applications.

2. Bi-Level Bottom-Up Computational Framework for Microstructural Analysis

In this section, we will provide the theoretical background of a seamless semi-analytical bi-level computational framework based on coupling the topology optimization with finite element analysis^[56] to achieve beam-level topology-optimized lattices with auxetic and non-auxetic configurations. We propose to integrate the concept of topology optimization with the design of periodic lattice networks under normal and shear modes following a unit cell based efficient computational approach. The effect of axial rigidity of the cell walls on the effective lattice-level elastic properties will be studied through two different models within the present framework by excluding and including the beam-level axial deformation components, while considering the bending deformation in both cases. Note that both of these models can be useful depending on the necessary level of computational efficiency and axial rigidity of the beams under consideration.

In essence, we aim to investigate the effects of the volume fraction of the topology-optimized cell walls along with other conventional microstructural parameters on the macro-scale effective elastic moduli. Here we will start with optimizing only the inclined members of the lattice (refer to Figure 1 for detailed lattice geometry and unit cell) and later extend the application toward the vertical members (note that for normal far-field stresses, if the axial deformation is neglected, only the slant

members of a hexagonal honeycomb contribute to the in-plane effective Young's moduli and Poisson's ratios). Under normal stress along direction-1, the vertical members do not deform even if the beams are not considered to be axially rigid, and hence they can be designed with a minimal amount of material distribution when only Young's modulus along direction-1 is of concern. However, for the multifunctional design of such lattices, where Young's modulus along direction-2 and shear modulus are also of interest, the vertical members also need to be designed optimally as proposed in this article.

Here we provide a brief explanation of the topology optimization scheme^[56] we have implemented at the beam level. Then we move to computations of effective elastic moduli of honeycomb lattices with topology-optimized cell walls (i.e., beams). The common parameters with which we deal with are the element dimensions, i.e., the height of the vertical member, the length of the inclined member, and the member thickness which are represented by h , l , and t , respectively. The cell angle is defined as θ (refer to Figure 1). The volume fraction of each member is represented by V_f . The Young's modulus and Poisson's ratio of the material used to prepare the lattice elements are E_0 and ν_0 (i.e., intrinsic material properties). The area and moment of inertia of the geometrical cross-section are defined as A and I . Under the applications of normal stress along direction-1 and -2 (refer to Figure 1 for the directions), and shear stress in the 12-plane, the topology-optimized beam-like cell walls undergo in-plane deformations which are computed using a finite element-based topology optimization code. The beam-level definitions including appropriate boundary conditions and the topology optimization concepts are explained in the supplementary sections SM1 and SM2, Supporting Information. We have proposed two separate beam models here (refer to Figure 2A–H), wherein we show that the half-length beam model is more generic (both axial and bending deformation can be considered) compared to the full-length beam model (only bending deformation can be considered).

Figure 2 gives a clear idea about the beam-level problem-solving approach that we deal with. As we have discussed earlier, our main objective is to enhance the specific lattice-level effective in-plane mechanical properties, like Young's moduli, Poisson's ratio, and shear modulus using topology-optimized members in addition to conventional unit cell based designs. The beam-level topology optimization must be carried out under proper boundary conditions and loading to the cell walls (i.e., beams). Generally beams with $t/l < 0.2$ do not show significant axial and shear deformation compared to bending^[8]; hence these components can be neglected in such cases. Here we have accounted for the cases of beam-level deformations both considering and neglecting axial deformations (while bending deformation considered in both cases). The shear deformation effect will be negligible in the current analysis as the cross-sections of the topology-optimized structural elements within a beam element will have very less transverse thickness compared to their lengths. Since, for topology-optimized beams, closed-form analytical formulae are not possible to be derived for the effective elastic properties of lattices like traditional literature (that considers solid beams),^[8] we resort to a semianalytical approach. First, we find out the transverse and axial deformations of topology optimized beams numerically (finite element analysis (FEA)

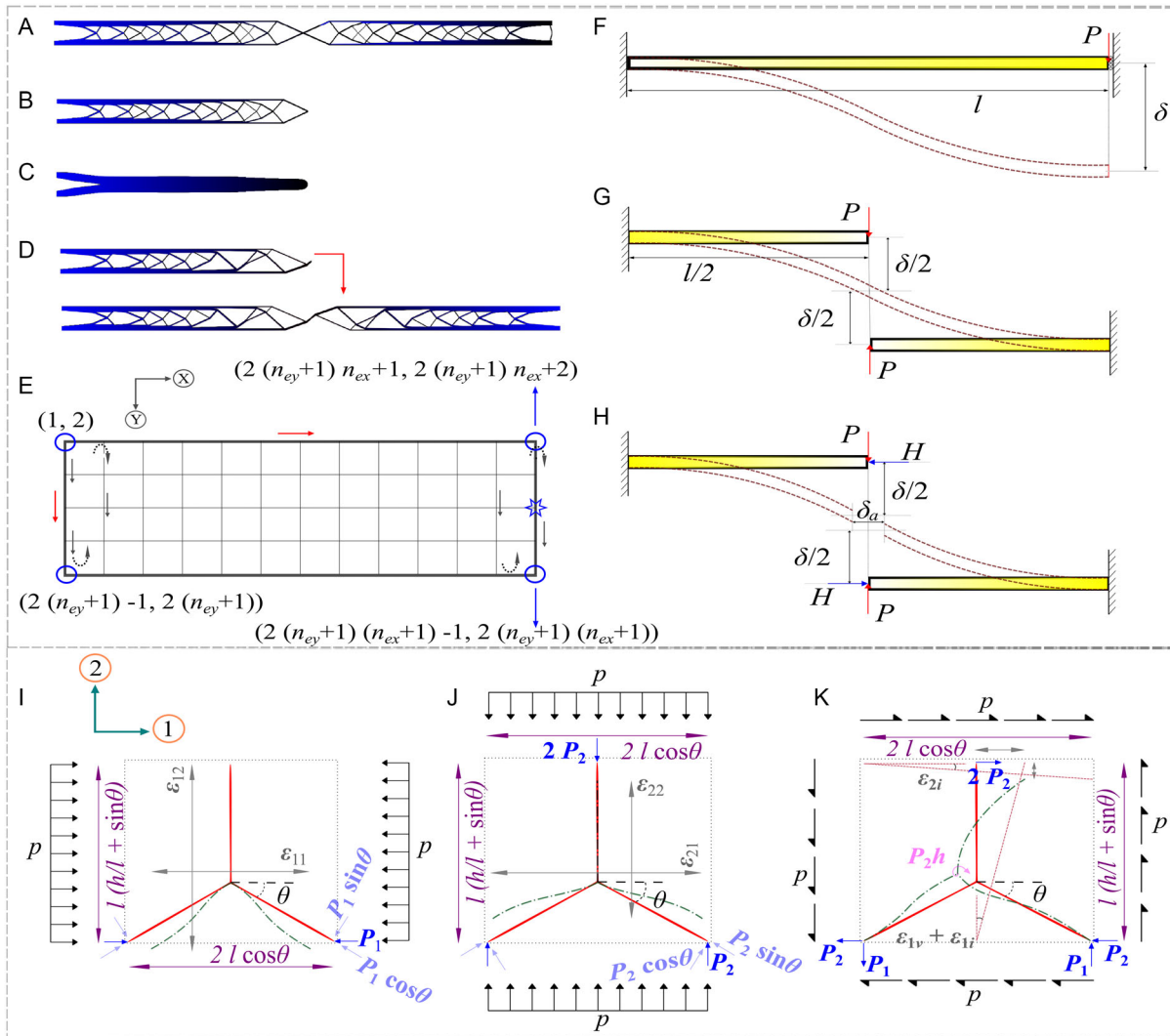


Figure 2. Beam models for optimized elementary level topologies and free body diagrams of the tri-member unit cells subjected to normal and shear stresses. A) Typical representation of a topology optimized beam that can be used in a full-length beam problem (one end clamped, the other end rotationally restrained, but free to have translations; subjected to a transverse point load at the end where the translation is allowed). B) Topology-optimized beam that can be used in a half-length beam problem (one end clamped and the other end free; subjected to a transverse point load at the free end). C) Topology-optimized beam that can be used in a half-length beam problem subjected to axial load only at the free end. D) Topology-optimized beam that can be used in a half-length beam problem subjected to both transverse and axial load at the free end. Along with this half-length beam, a full-length beam that can be generated by symmetrical replication is shown below. E) 2D beam element represented through square finite elements. A succession of nodes from (1, 2) is marked on the beam. F) Representation of a typical full-length beam problem with proper boundary and loading conditions. G) Representation of two symmetrically opposite typical half-length beam problems with proper boundary and loading conditions such that the overall analysis becomes equivalent to a full-length beam problem (only under transverse loading). H) Representation of two symmetrically opposite typical half-length beam problems with both transverse and axial loading. Note that such topology-optimized half-length and full-length beams are used for further lattice-level analyses. The half-length beam model can account for the effect of both bending and axial deformations, while the full-length beam model can account for only bending deformation. I–J) A typical unit cell under normal loading in directions 1 and 2, respectively. x and y in strain (longitudinal: $x = y$, lateral: $x \neq y$) ϵ_{xy} in these two free body diagram (FBD) indicate loading direction and deflection direction. K) A typical unit cell under shear loading. The first subscript (1 or 2) in the shear strain represents the loading direction and the second subscript is the member, i.e., i for the inclined member and ν for the vertical member.

model developed in the framework of the density optimization method with an overlay of the level set method), which are used thereby in an analytical framework to obtain the effective elastic properties at the lattice level.

In this context, it can be noted that once a member becomes topology optimized, we can only define the overall material

distribution by V_f . The way material is distributed within the spatial domain of the beam is taken care of by the topology optimization algorithm. Figure 2A–D shows typical topology-optimized beams for example. The value of V_f decides how much of the rectangular cross-section will be filled by the intrinsic material at different locations along the length of the beam. Under

supplementary section SM1, Supporting Information, the finite element framework for topology optimization^[56] is explained that has been used to compute load-deformation behaviors of topology-optimized beams here. After discussing the topology optimization concepts, we have focused on two different boundary conditions of the beams with half and full lengths (refer to supplementary section SM2, Supporting Information) that would be necessary for subsequent lattice-level property characterization. The beams are further utilized for analyzing unit cell level deformations and strains (refer to supplementary section SM3, Supporting Information). The free-body diagrams for the trimember unit cells (continuous red) subjected to normal and shear loading of p are shown in Figure 2I–K in a domain of size $l(h/l + \sin \theta) \times 2l \cos \theta$. The deformed cells (dashed green) are correspondingly represented and the final deformed lengths in directions 1 and 2 are shown using longitudinal, lateral, or shear strains. Within the framework of the unit cell approach (refer to Figure 2I–K), the beam-level deformations are utilized subsequently to compute the lattice-level effective elastic moduli as (scaled and nondimensionalized)

$$E_1 = \frac{p}{E_0(\rho_s)^3 \varepsilon_{11}} \quad (1)$$

$$E_2 = \frac{p}{E_0(\rho_s)^3 \varepsilon_{22}} \quad (2)$$

$$\nu_{12} = -\frac{\varepsilon_{12}}{\varepsilon_{11}} \quad (3)$$

$$\nu_{21} = -\frac{\varepsilon_{21}}{\varepsilon_{22}} \quad (4)$$

$$G_{12} = \frac{1}{E_0(\rho_s)^3} \left(\frac{\varepsilon_{1i} + \varepsilon_{2i}}{p} + \frac{\varepsilon_{1v}}{p} \right)^{-1} \quad (5)$$

A detailed derivation of the aforementioned formulae along with the expressions for strain components (under the application of far-field stress p) is given in supplementary section SM3, Supporting Information. The results of specific elastic moduli are obtained here in a nondimensional form, by dividing the respective values with a factor $E_0(\rho_s)^3$ as per standard literature.^[8] Relative density ρ_s in the denominator gives an understanding of the increase or decrease in the elastic moduli along with the corresponding change in relative density. Poisson's ratios, being the ratio of strains, are already normalized.

Relative densities of lattices with topology-optimized inclined members only (ρ_{1s}) and topology-optimized inclined and vertical members both (ρ_{2s}) are given by the following two equations, respectively.

$$\rho_{1s} = \frac{\left(\frac{h}{l} + 2V_f\right)^{\frac{1}{2}}}{2 \cos \theta \left(\frac{h}{l} + \sin \theta\right)} \quad (6)$$

$$\rho_{2s} = \frac{V_f \left(\frac{h}{l} + 2\right)^{\frac{1}{2}}}{2 \cos \theta \left(\frac{h}{l} + \sin \theta\right)} \quad (7)$$

In the current article, we use ρ_s in general equations, wherein depending on the type of optimization we can input the values of either ρ_{1s} or ρ_{2s} . For a detailed discussion on relative densities, refer to the supplementary section SM3.1, Supporting Information.

2.1. Summary

This section proposes a unit cell based semianalytical computational approach for evaluating the elastic properties of topology-optimized architected materials. The detailed derivation of each stage of the bottom-up algorithm is provided in the supplementary material. Supplementary section SM1, Supporting Information, provides the computational and theoretical backgrounds of finite element based topology optimization, while SM2, Supporting Information, provides a comprehensive description of the loading and boundary conditions of half-length and full-length beam models, which constitute the lattice. Subsequently, SM3, Supporting Information, shows the computational framework for obtaining the lattice-level effective elastic properties through the deformation behavior of the topology-optimized beam elements.

3. Results and Discussion

3.1. Twofold Validation of the Computational Framework

As computations of the lattice-level effective elastic moduli depend on deformation characteristics of the topology-optimized cell walls (i.e., beams), the topology optimization based beam model of the present framework is validated first with a commercial finite element tool in terms of deformation characteristics of topology-optimized beam. Subsequently, before investigations of the effect of volume fraction in the topology-optimized cell walls at the lattice level, the effective elastic moduli of lattices are also validated with analytical solutions considering the special cases with fully solid cell walls.^[8] The twofold validation study (beam-level and lattice-level) will provide adequate confidence in the present framework for estimating the effective elastic moduli of lattices with topology-optimized cell walls. Following that, the effects of the volume fraction of topology-optimized cell walls along with other conventional microstructural parameters on the effective elastic moduli would be presented. Due to the requirement of high computational time, we were unable to collect more data points for each of the curves while presenting a detailed investigation accounting for a range of design parameters. However, we have made sure that the trends are unaltered and a representation of the actual behavior.

3.1.1. Beam-Level Validation

As described in supplementary sections SM2 and SM3, Supporting Information, our framework has three different models at the elementary beam level, namely, the full-length beam problem under transverse loading, the cantilever model problem under transverse load only, and the half-length beam problem under combined transverse-axial loading. The three-beam problems are solved through the FEA-based topology optimization framework (refer to supplementary section SM1, Supporting Information) for different volume fractions V_f and thickness ratio t/l , and the deformation characteristics along with the topology-optimized shapes are obtained. For numerical demonstration, the intrinsic material is chosen as structural steel with Young's modulus value of 200 GPa and Poisson's ratio value of 0.3. The beam-level load is taken as the load under a lattice-level stress value of 0.05 MPa. Variations of the specific stiffness

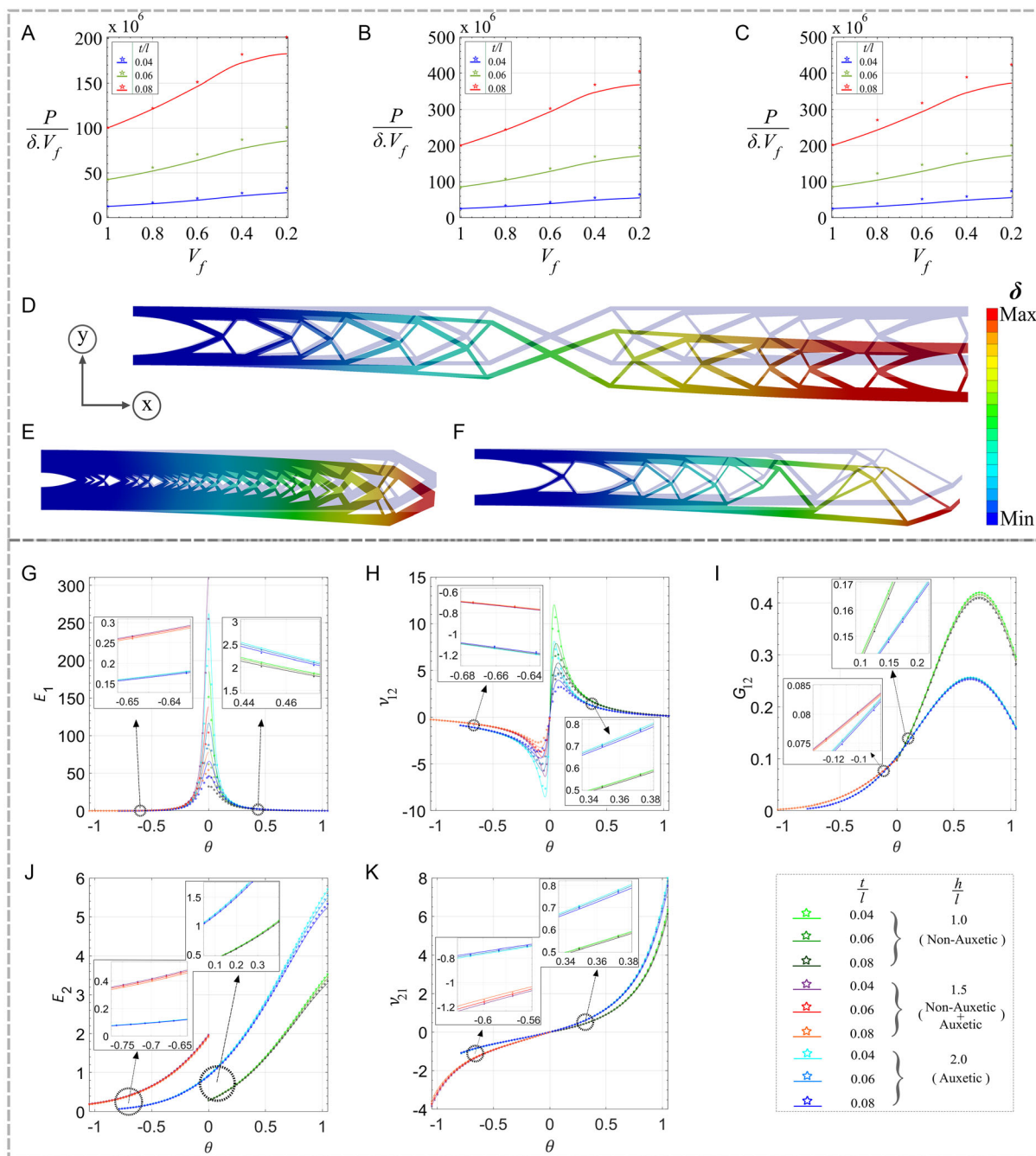


Figure 3. Beam-level and lattice-level validations. Variations of specific transverse stiffness ($P/\delta V_f$) (in N m^{-1}) is plotted with change in volume fraction V_f for different t/l ratios. The solid lines represent the results from the topology optimization code within the present framework whereas the markers show the results using a commercial FEA tool. A,D) Full-length beam level results with optimum topology using support settlement boundary condition under transverse load only. B,E) Half-length beam level results with optimum topology using cantilever boundary conditions under transverse load only. C,F) Half-length beam level results with optimum topology using cantilever boundary conditions under combined axial and transverse load. Figures D–F) give a general idea regarding the resulting typical topology-optimized beams and their deflections when subjected to the prescribed loading and boundary conditions. G–K) Validation of lattice level nondimensional specific elastic properties (E_1 , E_2 , v_{12} , v_{21} and G_{12}) with cell angle θ (in radian), h/l and t/l , taking volume fraction as 1. The Young's moduli and shear modulus are normalized by $E_0(\rho_s)^3$. The solid lines represent analytical results^[8] whereas the markers represent the results from the present framework.

$\frac{P}{\delta V_f}$ with the volume fraction V_f are shown through solid lines in **Figure 3A–C** for the three beam problems, where P is the transverse loading in N and δ is the transverse deformation in m unit.

The figure clearly shows that specific stiffness $\frac{P}{\delta V_f}$ increases with the decrease in volume fraction V_f and such increment depend upon t/l ratio. The topology-optimized beam configurations as

obtained from the FEA-based topology optimization framework are presented in Figure 3D–F, respectively, corresponding to the three types of problems. The topology-optimized beam configurations for different volume fractions are modeled in the framework of a commercial FE tool^[58] and the corresponding deflections are computed, which in turn give specific stiffness $\frac{P}{\delta V_f}$. The specific stiffness values obtained from the FE tool are plotted against the volume fraction and shown through markers in Figure 3A–C. An excellent agreement can be noticed between the results of the FEA code and that of the commercial FE tool, corroborating further confidence in the numerical results.

As observed in Figure 3A,B, the transverse stiffness values for the half-length beam problem are double for those of the full-length beam problem when the only transverse load is considered. The deformation characteristics are further reinforced as discussed in Figure 2 (refer to supplementary section SM2, Supporting Information) that for application of the same transverse load, a full-length beam when solved using support settlement boundary condition shows two times the deformation shown by a half-length beam solved as a half-length beam problem for a particular value of V_f (note that it has already been shown analytically in supplementary section SM2, Supporting Information for solid beams with $V_f = 1$; here we show that this statement is true of any V_f). However, as the effect of axial load is comparably less, we can get almost similar stiffness values under the combined transverse and axial load as observed in Figure 3C. As observed from Figure 3A–C, the results from the FEA tool match with the FEA-based topology optimization framework for a higher volume fraction V_f . But with the decrease in volume fraction V_f , the difference between them increases. Such variations in the results are due to the accuracy in modeling the complicated beam topology in the FEA tool from the raster image the optimization code gives. Due to the huge time requirement, we have restricted the n_{ey} value to 60 units (defined in SI units) which is the beam thickness, t . The length of the inclined and vertical members is controlled by t/l and h/l ratio. A clear raster image with more elements (pixels) will help to extract the edges for the topology-optimized beam in a more efficient manner. However, within the scope of the article, the comparison studies presented in Figure 3A–C can be considered satisfactory. Our aim to increase the specific stiffness at lower V_f is achieved through topology optimization of the beam as shown in the figures.

Two scales involved in the proposed lattices are at: 1) unit-cell-level geometry, and 2) beam-level topology. At the unit cell level, we have specific dimensions of the beam lengths, thickness, and angles of the hexagon. However, at the beam level, the microstructural topology is primarily defined by volume fraction (refer to Figure S7, Supporting Information) and pixel size. Depending on the volume fraction and pixel size, the spatially varying beam-level architecture is obtained following topology optimization. It is possible to define a scale ratio by taking a ratio of the dimension of the pixels and the thickness of a beam. Note that knowing the thickness, and dimension of the vertical and slant members can be evaluated from t/l and h/l ratios. As per the proposed definition, we have used a scale ratio of 1/60 in the present study. Reducing the scale ratio further will lead to a better topology-optimized structure with smoother boundaries, but at the cost of more computational intensiveness. In the following

subsections, we use the beam-level deformation with topology-optimized configurations for evaluation of the lattice-level effective mechanical properties, wherein the unit cell geometries play additional interactive roles along with the beam topologies.

3.1.2. Lattice-Level Validation

Followed by the beam-level validation, the lattice-level effective elastic moduli computed by the present framework are compared with the analytical results from the literature.^[8] For this purpose, we use the cantilever half-beam model to evaluate the effective elastic moduli in the current approach. However, such validation can be only carried out for solid members in the lattice, i.e., taking V_f as 1 since this case is only available in the existing literature. Variations of the effective elastic moduli concerning different configurations of cell angle θ along with h/l and t/l ratios are shown in Figure 3G–K. It is to be noted that geometric feasibility should be taken care of while designing the lattices with negative cell wall angle. For example in the current article, when auxetic cases are considered with $h/l = 1.5$ and cell wall angle, $\theta = 60^\circ$, the geometrical feasibility condition, $h/l > 2\sin\theta$ is not fulfilled. Hence we have not shown the corresponding plots. The solid lines represent the analytical results^[8] whereas the markers show the results computed by the present framework. For the cases when θ is close to zero, the effective elastic moduli obtained under loading in direction 1 become completely dependent on the axial deformation. Since axial rigidity is much higher compared to bending rigidity, the values of such effective elastic moduli shoot up near $\theta = 0$. For higher θ values both on the positive and negative side, the differences in the curves become almost negligible; hence zoomed views are shown through insets in the plots for all the cases. The insets show the variations in the effective elastic moduli results with h/l and t/l ratios.

Variations of E_1 and E_2 with cell angle θ as shown in Figure 3G,J indicate that the plot for E_1 is similar to a Gaussian peak, while the nature of E_2 is likely to have a sigmoid curvature if we observe using best fit for the range we have used. As observed in Figure 3H,K, a plot for ν_{12} is similar to two log-normal curves at both signs of θ , while ν_{21} shows an inflection point near the origin which increases and decreases exponentially for higher θ values on both sides of the origin. From Figure 3I, we observe that G_{12} increases up to θ equal 0 for auxetic configurations. But for the non-auxetic cases, a peak is observed at 0.65 radians. In general, the lattice level results considering volume fraction 1 show satisfactory alignment with respect to the results from established literature, corroborating the validity of the proposed semi-analytical framework.

This is a computational and semianalytical paper, where extensive computational validation is provided at two different levels with separate finite element analyses and the available literature: 1) at the beam level and 2) at the lattice level. It can be noted here that the effective elastic properties of hexagonal lattices with solid beam-like members ($V_f = 1$) have been experimentally validated in the literature.^[8] Since we have also compared the current results for $V_f = 1$ with the closed-form formulae given in ref. [8], it gives us adequate confidence in the lattice-level computational framework. In the following subsections, we present

numerical results demonstrating the capability of beam-level topology optimization for maximizing lattice stiffness under normal and shear modes of loading. Comprehensive numerical results would be discussed critically covering the entire spectrum of possibilities concerning the auxetic and non-auxetic behavior of the lattices in an expanded design space, demonstrating multifunctional property enhancement and programmability.

3.2. Mechanical Characterization of Lattices with Micro-Architected Inclined Beams Only

The results presented in this subsection are concerning the cases when we apply topology optimization only to the inclined members of the unit cell comprising the lattices. Note that this case is relevant considering the fact that the inclined members mostly contribute to the lattice-level deformation through bending. When axial deformations are neglected, there is almost no role in the lattice-level strains for the vertical members under normal remote stresses, except for forming the geometry of the unit cells. However, it should be noted that the vertical members contribute to bending deformation significantly under remote shear stress, for which the vertical members also become crucial. For this particular set of simulations, the vertical members are kept fully solid to avoid any extra computational cost of topology optimization. Hence to calculate the specific lattice properties, we will use the specific density, ρ_{1s} as given in Equation (6). The effective elastic moduli are computed using the full-length beam model and half-length cantilever beam model of the proposed framework as presented in the following subsections.

3.2.1. Effective Young's Moduli and Poisson's Ratios Based on Full-Length Beam Problem

In this subsection, we investigate the variation of specific Young's moduli E_1 and E_2 with decreasing volume fraction V_f from 1. We aim to make sure that by performing topology optimization on the solid beam, we can enhance E_1 and E_2 significantly. The parametric study has been performed by changing the geometrical properties like h/l , t/l and cell angle, θ . Figure 4A–F gives a clear picture that for the non-auxetic lattice, and how both the specific Young's moduli show a steep rise while we decrease the volume fraction performing topology optimization on the inclined cell walls. When h/l ratio equals 1.5 for the non-auxetic lattice, we find the steepness of the plot decreases after V_f reaches 0.4. Similar behavior is observed for the auxetic lattices in Figure 4G–F where h/l is 1.5. For h/l the ratio increasing up to 2 in Figure 4H–L, a decrement of E_1 and E_2 is observed when V_f is reduced from 0.4. This indicates high deflection that may deform the overall lattice significantly. Hence, we can optimize the beams up to a higher V_f like 0.5 keeping this in mind. Also, for all the cases, we observe that by lowering t/l ratio, the specific Young's moduli increase. It is also observed that for both the auxetic and non-auxetic cases, the magnitude of E_2 is always on the higher side than E_1 for any value of t/l , h/l or θ .

Figure S1A–L, Supporting Information, shows the variation of Poisson's ratios (ν_{12} and ν_{21}) with decreasing volume fraction. ν_{12} remains constant with change in V_f and t/l whereas magnitude-wise, ν_{21} increases marginally from a lower rate to higher rate as

we reduce V_f . The marginal variation (or invariance) of Poisson's ratios when considering only the bending deformation of the hexagonal lattices is consistent with the established literature.^[8,21] This indicates that the Poisson's ratios in this case are dependent on only the unit cell level geometries rather than the beam-level topology and beam-level physics. However, the inclusion of the effect of axial deformation would change this inference slightly, as discussed later in this article. For all the cases, we observe that by lowering the t/l ratio, the Poisson's ratio increases, while there also exists a definite dependence on the cell angle as well. The negative cell angles lead to an auxetic behavior, i.e., negative Poisson's ratio. We have confirmed that for any particular case, $E_2\nu_{12} = E_1\nu_{21}$ ^[57] is satisfied. This provides further confidence to the numerical results presented here.

3.2.2. Effective Shear Modulus G_{12} Based on Full-Length Beam Problem

Effect of volume fraction V_f on specific shear moduli G_{12} is investigated in this subsection to enhance G_{12} . Variations of G_{12} with volume fraction V_f for the considered microstructural parameters (h/l , t/l and θ) are shown in Figure 5A–C. The figure gives a clear picture that for the non-auxetic lattice, the specific shear modulus shows a rise with a decreasing rate while we decrease the volume fraction through topology optimization on the inclined cell walls. For h/l ratio increasing up to 2 in Figure 5D–F, a decrement of G_{12} is observed when V_f is reduced beyond 0.4. Also, for all the cases, we observe that by lowering the t/l ratio, the specific shear modulus increases. It is also observed that for both the auxetic and non-auxetic cases, the magnitude of G_{12} increases for a greater value of h/l .

3.2.3. Effective Young's Moduli and Poisson's Ratios Based on Half-Length Beam Problem

The line plots in Figure S2, Supporting Information represent the case when we solve the problem using a cantilever boundary condition considering both the transverse and axial deformations at the beam level. The markers in the figures represent the effective elastic moduli results for the case when we consider transverse loading only for the cantilever boundary condition (these results are provided to give a clear sense of the individual contribution of axial deformations). Up to $V_f = 0.6$, the difference is negligible and the marker positions are slightly higher indicating that accounting for the axial force, reduces the value of specific Young's moduli. But this trend is not similar at $V_f = 0.2$. The complex topology optimization process leads to a result for which accounting for the axial loading reduces the moduli values.

For the Poisson's ratios (ν_{12} and ν_{21}) as shown in Figure S3, Supporting Information, we can identify the difference between considering and neglecting axial deformations more clearly as the values lie within a very small range. The nature of plots for the cases are similar but there is no regular trend as the results are dependent upon the topology optimization concerning a range of parameters. But we find the markers to be present at a slightly lower magnitude and this difference is more at higher V_f , which indicates accounting axial load lowers the Poisson's ratio magnitude. Note that the observation concerning

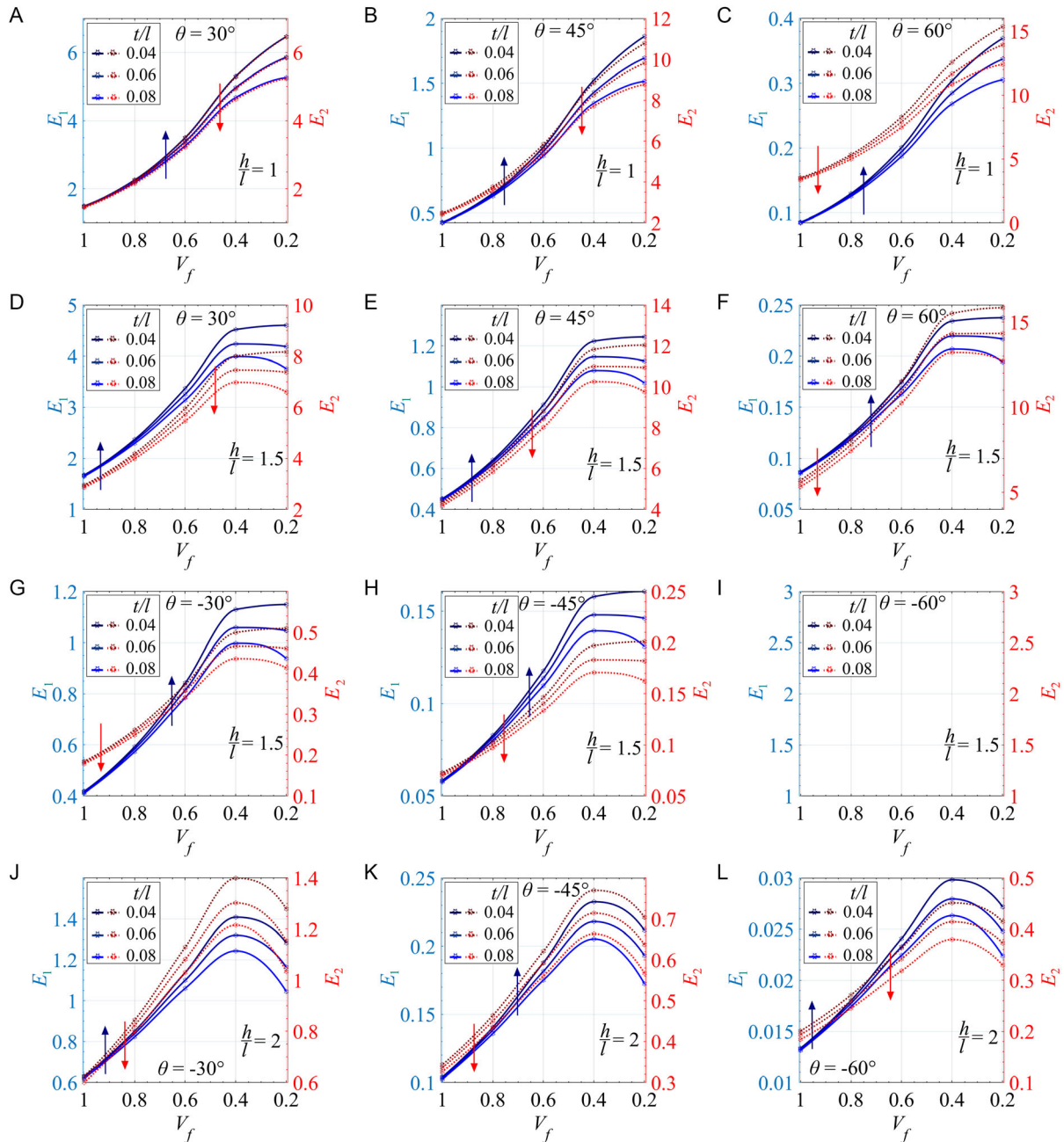


Figure 4. Specific Young's moduli for lattices with different unit cell geometries considering topology-optimized inclined cell walls (with only bending deformation). Variations of specific Young's moduli E_1 and E_2 with change in volume fraction V_f of the topology optimized cell walls constituting the overall lattice. The parametric study includes variation in the values of θ , h/l and t/l . The results are plotted considering only the transverse loading on the beam elements. A–F) θ ranging in the positive domain indicating non-auxetic properties. G–L) θ ranging in the negative domain indicating auxetic properties. Here the topology optimization has been carried out only for the inclined members of the unit cell. Nondimensional schemes are adopted as per Equation (1) and (2).

the dependence of Poisson's ratio on the beam-level topology and mechanics when the axial deformation is considered along with bending deformation is consistent with established literature on hexagonal lattices.^[59] For obtaining this set of results we have considered the topology optimization in the slant beams only; however, when we will consider the topology optimization in both slant and vertical beams including both the bending and

axial deformations (as presented later in this article), the effect of V_f on ν_{21} would be much more prominent.

For practical purposes, the difference that we get for either Young's moduli or Poisson's ratio is rather minor. Hence, if we use Figure 2A,D as topology-optimized cell walls, we will not encounter any significant difference in results. It could, however, be kept in mind that consideration of axial deformations

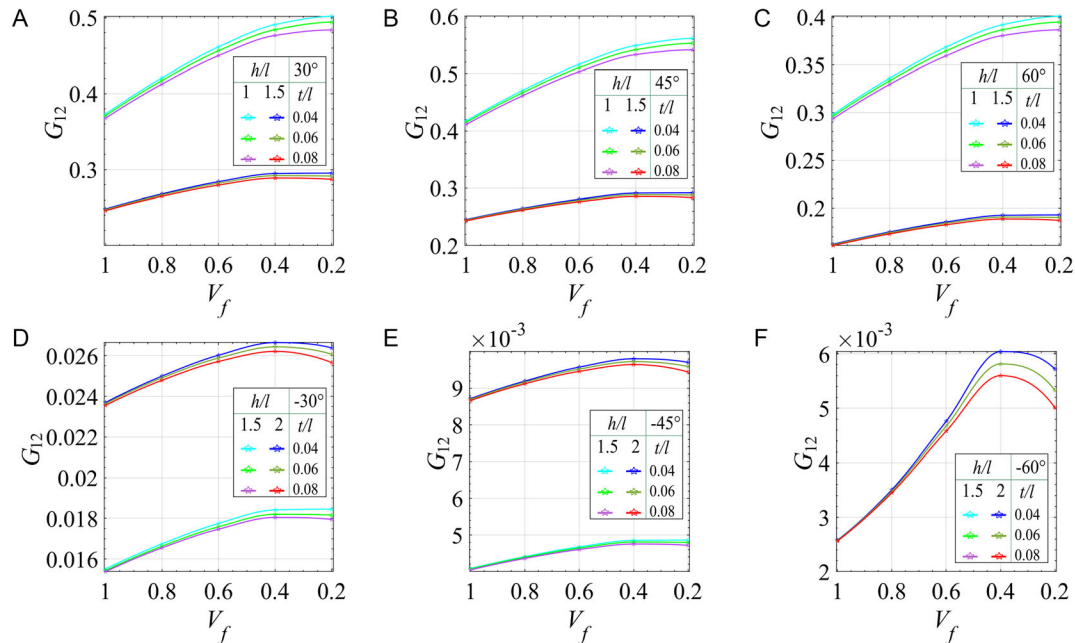


Figure 5. Specific shear modulus for lattices with different unit cell geometries considering topology-optimized inclined cell walls (with only bending deformation). Variations of specific shear modulus G_{12} with change in volume fraction V_f of the topology optimized cell walls constituting the overall lattice. The parametric study includes variation in the values of θ , h/l and t/l . The results are plotted considering only the transverse loading on the beam elements. A–C) θ ranging in the positive domain indicating non-auxetic properties. D–F) θ ranging in the negative domain indicating auxetic properties. Here the topology optimization has been carried out only for the inclined members of the unit cell. Nondimensional schemes are adopted as per Equation (4).

provides more accurate results at the cost of more computational expenses. As per the proposed models, the effect of axial deformation can only be considered in the half-beam analysis, while the transverse bending analysis can be carried out by both the half- and full-beam models. In general, the full-beam analysis is more expensive than the half-beam analysis, while combined bending and axial analysis in the half-beam model is more expensive than the analysis considering only bending deformation. Such comments are valid for all the elastic moduli under consideration in this work and appropriate decisions regarding the analysis approach that should be taken based on justifiable engineering judgments.

3.2.4. Effective Shear Modulus G_{12} Based on Half-Length Beam Problem

Variations of specific shear modulus G_{12} with volume fraction for the considered geometric parameters are shown in Figure S4, Supporting Information. The solid or dashed lines represent the case when we solve the problem using cantilever boundary conditions but the beam is subjected to both transverse and axial loading. The markers in the figures represent the coordinates for the case when we solve the problem using cantilever boundary conditions but the beam is subjected only to transverse loading. The trends of variations of specific shear modulus captured by the model including axial deformation are similar to those of excluding axial deformation. As the magnitude of specific shear modulus, G_{12} values as shown in Figure S4, Supporting Information, lie within a higher range, it is difficult

to identify the minor differences in the values, which can be only seen at lower volume fractions. However, the comments made in the preceding subsection regarding half- and full-length beams (and considering or neglecting axial deformations) for Young's moduli and Poisson's ratios remain valid for the shear modulus as well.

3.3. Mechanical Characterization of Lattices with Micro-Architected Inclined and Vertical Beams

So far in this article, we have presented results where we considered topology optimization in the slant beams only. However, a design considering topology optimization in the vertical beams, in addition, would lead to improvement of the mechanical properties further. The results presented in this subsection consider the cases when we apply topology optimization to both the inclined and vertical members of the unit cell comprising the lattice. Hence to calculate the specific lattice properties, we will use the specific density, ρ_{2s} as given in Equation (7). As the vertical members deform only under normal stress along direction-2 and shear mode of applied remote stress, we only deal with specific Young's modulus E_2 , ν_{21} and specific shear modulus G_{12} here. Under normal stress along direction-1, the vertical members do not deform, and hence the vertical cell walls corresponding to E_1 and ν_{12} are kept solid as of the previous subsection. As we are optimizing the members for both axial and transverse loading here, we are bound to use the cantilever boundary conditions. Variations of specific Young's modulus E_2 , ν_{21} , and specific shear modulus G_{12} with volume fraction of the

topology-optimized cell walls are shown in **Figure 6** and S5, Supporting Information. From the figures, we can find a significant increment in the magnitudes of the specific moduli, which shows further reinforces the hypothesis of improving the

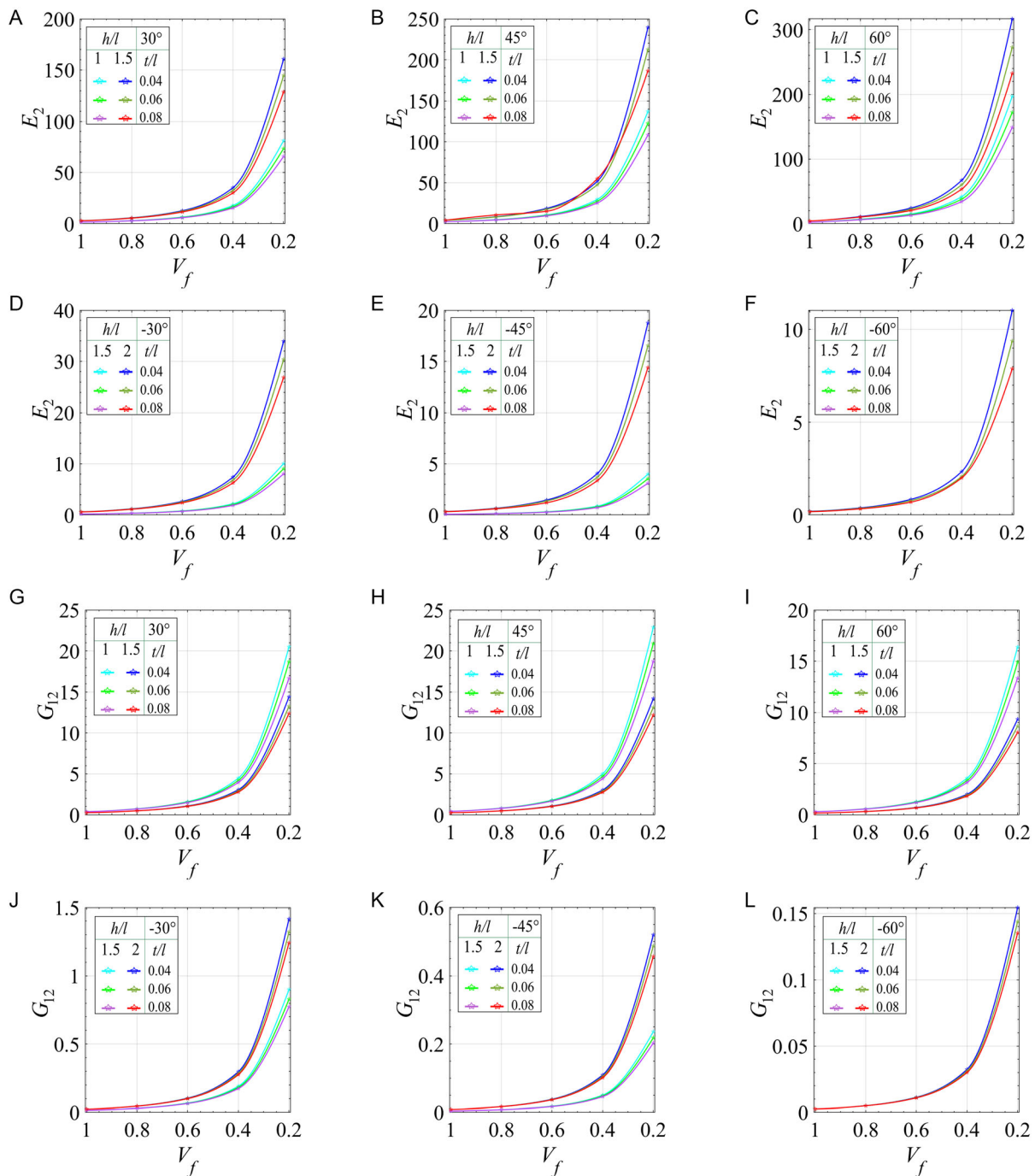


Figure 6. Specific Young's moduli and shear modulus for lattices with different unit cell geometries considering topology-optimized vertical and inclined cell walls (with both bending and axial deformations). Variations of specific Young's modulus E_2 and specific shear modulus G_{12} are plotted with a change in volume fraction V_f of the topology-optimized cell walls constituting the overall lattice. The parametric study includes variation in the values of θ , h/l , and t/l . The results are plotted using cantilever boundary conditions (half-length beam model) considering both transverse and axial loading on the beam elements. A–C) E_2 for θ ranging in the positive domain indicating non-auxetic properties. D–F) E_2 for θ ranging in the negative domain indicating auxetic properties. G–I) G_{12} for θ ranging in the positive domain indicating non-auxetic properties. J–L) G_{12} for θ ranging in the negative domain indicating auxetic properties. Here the topology optimization has been carried out both for the inclined and vertical members of the unit cell. The adopted nondimensional schemes are as per Equation (2) and (4).

specific mechanical properties by optimizing both the vertical and slant members.

3.3.1. Effective Young's Moduli and Poisson's Ratios Based on Half-Length Beam Problem

The parametric study on the effects of volume fraction V_f and lattice parameters θ , h/l , and t/l as shown in Figure 6A–F gives a clear picture for non-auxetic lattices as to how the specific young's modulus, E_2 shows a rise with an increasing rate while we decrease the volume fraction for topology optimization in both the inclined and vertical members. It is also observed that for both the auxetic and non-auxetic cases, the magnitude of E_2 increases more for the higher value of h/l . While at higher volume fractions the rate of increment is low, after V_f decreases beyond 0.4, we get an exceptional rise in E_2 .

We have further investigated the variation of Poisson's ratio ν_{21} with decreasing volume fraction, V_f . The parametric study has been performed by changing the geometrical properties like h/l , t/l , and cell angle, θ . Figure S5, Supporting Information gives a clear picture of the lattices (both auxetic and non-auxetic) as to how ν_{21} shows a rise in magnitude with an increasing rate while we decrease the volume fraction considering topology optimization of both the inclined and vertical members. It is also observed that for both the auxetic and non-auxetic cases, the magnitude of ν_{21} increases for a greater value of h/l . After decreasing V_f beyond 0.4, we get a significant rise for ν_{21} on further decreasing the volume fraction. Note that the observation concerning the strong dependence of Poisson's ratio on the beam-level topology and mechanics when the axial deformation is considered along with bending deformation is consistent with the established literature on hexagonal lattices.^[59]

3.3.2. Effective Shear Modulus G_{12} Based on Half-Length Beam Problem

In this subsection, we have investigated the enhancement of specific shear moduli, G_{12} with decreasing volume fraction, V_f . The parametric study has been performed by changing the geometrical properties like h/l , t/l and cell angle, θ . Figure S5G–L, Supporting Information gives a clear picture of the non-auxetic lattices as to how the specific shear modulus shows a rise with an increasing rate while we decrease the volume fraction considering topology optimization of both the inclined and vertical members. It is also observed that for both the auxetic and non-auxetic cases, the magnitude of G_{12} increases for a greater value of h/l . After decreasing V_f beyond 0.4, we get a significant rise for G_{12} on further decreasing the volume fraction.

3.4. Specific Density of Bi-Level Micro-Architected Lattices

Since we focus on the specific lattice properties as functions of the volume fraction of topology-optimized cell walls, it is crucial to investigate how the volume fraction influences the lattice density. We have already discussed earlier the formulations for ρ_{1s} and ρ_{2s} in Equation (6) and (7). The value for ρ_{1s} is greater than ρ_{2s} as optimization of the vertical members reduces the solid volume further for the latter, reducing the magnitude of ρ_{2s} .

Variations of the relative lattice density with the volume fraction of the cell walls in association with the other conventional microstructural parameters are shown in Figure S6, Supporting Information. The numerical results reveal that specific density linearly increases with an increase in volume fraction V_f for a certain set of values of θ , h/l , and t/l . The slope of the lines increases with a rise in cell angle θ . Moreover, the increments in the slopes of the curves with t/l ratio indicate that the values of specific density are on the higher side for thicker beams. The numerical results presented in Figure S6, Supporting Information would allow the readers to find out the exact values of the elastic moduli furnished throughout the paper readily for different configurations.

4. Conclusions and Perspective

This article proposes a bi-level architecture for innovating extreme materials where besides having the conventional periodic lattice at an upper scale, the constituting beams at a lower scale are also topology optimized for most optimum material utilization. The coupled interaction of beam-level and lattice-level architectures enhances the specific elastic properties to a significant extent compared to the conventional lattices with solid beam networks, leading to ultra-lightweight multifunctional structural materials. Essentially, we integrate the concept of topology optimization with the design of periodic lattice networks under normal and shear modes following a unit cell-based efficient semi-analytical computational framework.

A systematic bottom-up approach has been undertaken here for the development of bi-level topology-optimized lattices. At the beam level, we propose the possibility of using two beam models with full-length and half-length along with appropriate boundary conditions to conform with the unit cell level periodic deformation behavior. The half-length beam model is capable of accounting for both the transverse and axial deformations (or only the bending deformation, if necessary), while the full-length beam model does not consider the effect of axial deformation. In general, the half-length beam model is less computationally expensive compared to the full-length beam model. However, consideration of axial deformation, even though it makes the predictions more accurate, adds up the computational cost due to additional axial topology optimization at the beam level. Normally the slant members are quite crucial in the deformation mechanics of hexagonal lattices. Thus, initially, we start with topology optimization of the slant members only to improve the mechanical behavior. However, the inclusion of the vertical members along with the slant members in the subsequent designs, leads to significantly higher transverse specific Young's modulus and shear modulus.

To garner adequate confidence in the outcome of this study, a two-level validation approach is adopted. At the beam level, we validate the responses of both half and full-length beams considering different volume fractions. It is established that the response of a half-length beam with appropriate boundary conditions can be tantamount to the response of a full-length beam. The half-beam model analysis leads to achieving a significant extent of computational efficiency due to a reduction in the physical optimization domain. At the lattice level, we validate the

elastic moduli with available literature for the case of volume fraction 1. After having adequate confidence in the proposed computational models through the beam- and lattice-level validations, we investigate the expanded coupled microstructural space exhaustively for enhancing the specific mechanical properties.

Insightful numerical results are presented covering the entire spectrum of possibilities concerning the auxetic and non-auxetic behaviour of the lattices in an expanded design space (interaction of optimum beam-level topology with intrinsic material properties and the unit cell level geometric parameters like thickness to length ratio (t/l), the ratio of the length of the vertical cell wall to the length of inclined member (h/l), and cell angle (θ)), demonstrating the capability of multifunctional property enhancement and programmability. The specific mechanical properties (Young's and shear moduli) can be enhanced up to 3 times for E_1 , 12.5 times for E_2 , and 10 times for G_{12} , when we perform topology optimization in both the inclined and vertical members of the unit cell comprising an overall non-auxetic lattice while reducing volume fraction to 0.5 from 1. For an auxetic lattice, the enhancement is up to 2.5 times for E_1 , 25 times for E_2 , and 20 times for G_{12} (note that we have presented results as a ratio of the elastic moduli and relative density to capture the net enhancement of mechanical properties normalized by weight). The numerical results further reveal an interesting interplay among the unit cell geometries and volume fraction, wherein a wide range of auxeticity (and Poisson's ratio, in general) can be achieved without changing the unit cell level geometry.

In general, the stiffness of a structure is controlled by the effective elastic moduli of structural materials. Recently architected lattice materials have drawn tremendous attention due to their enhanced mechanical performances in multifunctional applications (such as direction and mode-dependent static and dynamic behavior, impact resistance and energy absorption, stability control, and actuation) that can be realized through artificial micro-structuring. Since most of these multifunctional properties are linked to elastic moduli, enhancing the elastic moduli would have a significant impact on the structural behavior. Rapidly evolving capabilities of additively manufacturing complex microstructures have made the physical realization of lattice materials possible. However, the research area on the design of artificial microstructural configurations for the modulation of mechanical properties has become saturated lately due to extensive investigations in the field considering different possibilities of lattice geometry and beam-like network design. In this article, we have presented an innovative avenue at a more elementary level that can grow the microstructural space laterally for enhancing the effective elastic moduli. Seamlessly coupling the idea of topology optimization with unit cell design of periodic lattices has been the foundation to develop this new class of architected materials. The rich multifunctional properties of the proposed 2D microstructures make them ideal for the creation of innovative high-performance lightweight structural systems with multiobjective goals in a wide range of milli-, micro-, and nanometer-scale advanced applications. The conceptual development of bi-level microstructural design as proposed here, being generic in nature, can further be extended to other forms of lattices in 2D and 3D spaces.

Supporting Information

Supporting Information is available from the Wiley Online Library or from the author.

Acknowledgements

D.K., S.G., T.M. and S.N. contributed equally to this work, as written in the originally supplied version. D.K. acknowledges the financial support from the Ministry of Education, India, through a scholarship. S.N. acknowledges the Initiation grant received from the University of Southampton. T.M. would like to acknowledge the Initiation grant received from IIT Kanpur during the period of this research work.

Conflict of Interest

The authors declare no conflict of interest.

Author Contributions

T.M.: conceived the idea. D.K. and S.G.: prepared the results under the supervision of T.M. and S.N.: The final manuscript was written by all the authors.

Data Availability Statement

The data that support the findings of this study are available from the corresponding author upon reasonable request.

Keywords

auxetic metamaterials, bi-level topology-architected lattices, extreme specific stiffness, lattice materials, tunable elastic moduli

Received: September 28, 2022

Revised: November 20, 2022

Published online:

- [1] H. N. Wadley, *Philos. Trans. R. Soc. A* **2006**, 364, 31.
- [2] A. G. Izard, R. F. Alfonso, G. McKnight, L. Valdevit, *Mater. Des.* **2017**, 135, 37.
- [3] K. E. Evans, A. Alderson, *Adv. Mater.* **2000**, 12, 617.
- [4] X. Chen, Q. Ji, J. Wei, H. Tan, J. Yu, P. Zhang, V. Laude, M. Kadic, *Int. J. Mech. Sci.* **2020**, 169, 105288.
- [5] T. Frenzel, V. Hahn, P. Ziemke, J. L. G. Schneider, Y. Chen, P. Kiefer, P. Gumbsch, M. Wegener, *Commun. Mater.* **2021**, 2, 4.
- [6] A. Sinha, T. Mukhopadhyay, *iScience* **2022**, 25, 104649.
- [7] B. Isanaka, T. Mukhopadhyay, R. Varma, V. Kushvaha, *Acta Mater.* **2022**, 239, 118226.
- [8] L. Gibson, M. Ashby, *Cellular Solids: Structure and Properties*, Cambridge University, Cambridge **1999**.
- [9] Z. Hashin, S. Shtrikman, *J. Mech. Phys. Solids* **1963**, 11, 127.
- [10] A. A. Zadpoor, *Mater. Horiz.* **2016**, 3, 371.
- [11] Y. Miyazawa, H. Yasuda, H. Kim, J. H. Lynch, K. Tsujikawa, T. Kunimine, J. R. Raney, J. Yang, *Commun. Mater.* **2021**, 2, 110.
- [12] T. Mukhopadhyay, D. Kundu, *Adv. Eng. Mater.* **2022**, 24, 2101183.
- [13] T. Mukhopadhyay, A. Mahata, S. Naskar, S. Adhikari, *Adv. Theor. Simul.* **2020**, 3, 2000129.

- [14] S. Kumar, S. Tan, L. Zheng, D. M. Kochmann, *npj Comput. Mater.* **2020**, *6*, 73.
- [15] Y. Chen, T. Li, F. Scarpa, L. Wang, *Phys. Rev. Appl.* **2017**, *7*, 024012.
- [16] T. Mukhopadhyay, A. Mahata, S. Adhikari, M. A. Zaeem, *Nanoscale* **2018**, *10*, 5280.
- [17] S. Malek, L. Gibson, *Mech. Mater.* **2015**, *91*, 226.
- [18] S. Malekmohammadi, L. J. Gibson, *Mech. Mater.* **2015**, *91*, 226.
- [19] L. R. Meza, G. P. Phlipot, C. M. Portela, A. Maggi, L. C. Montemayor, A. Comella, D. M. Kochmann, J. R. Greer, *Acta Mater.* **2017**, *140*, 424.
- [20] S. Wehmeyer, F. W. Zok, C. Eberl, P. Gumbsch, N. Cohen, R. M. McMeeking, M. R. Begley, *J. Mech. Phys. Solids* **2019**, *133*, 103693.
- [21] A. Singh, T. Mukhopadhyay, S. Adhikari, B. Bhattacharya, *Int. J. Solids Struct.* **2021**, *208*, 31.
- [22] T. Mukhopadhyay, S. Adhikari, A. Batou, *Int. J. Mech. Sci.* **2019**, *150*, 784.
- [23] T. Mukhopadhyay, S. Naskar, S. Adhikari, *Extreme Mech. Lett.* **2020**, *40*, 100934.
- [24] A. Singh, T. Mukhopadhyay, S. Adhikari, B. Bhattacharya, *Smart Mater. Struct.* **2022**, *31*, 125005.
- [25] M. Mirzaali, H. Pahlavani, E. Yarali, A. Zadpoor, *Sci. Rep.* **2020**, *10*, 11488.
- [26] A. Roy, K. Gupta, S. Naskar, T. Mukhopadhyay, S. Dey, *Mater. Today Commun.* **2021**, *26*, 102021.
- [27] Y. Chandra, T. Mukhopadhyay, S. Adhikari, Ł. Figiel, *Nanotechnology* **2020**, *31*, 145705.
- [28] T. Mukhopadhyay, A. Mahata, S. Adhikari, M. A. Zaeem, *Sci. Rep.* **2017**, *7*, 15818.
- [29] T. Mukhopadhyay, J. Ma, H. Feng, D. Hou, J. M. Gattas, Y. Chen, Z. You, *Appl. Mater. Today* **2020**, *19*, 100537.
- [30] H. Wang, D. Zhao, Y. Jin, M. Wang, T. Mukhopadhyay, Z. You, *Appl. Mater. Today* **2020**, *20*, 100715.
- [31] A. Walker, T. Stankovic, *Commun. Mater.* **2022**, *3*, 4.
- [32] M. J. Mirzaali, A. Ghorbani, K. Nakatani, M. Nouri-Goushki, N. Tümer, S. J. P. Callens, S. Janbaz, A. Accardo, J. Bico, M. Habibi, A. A. Zadpoor, *Adv. Mater.* **2021**, *33*, 2008082.
- [33] H. M. Kolken, A. Zadpoor, *RSC Adv.* **2017**, *7*, 5111.
- [34] L. Yang, O. Harrysson, H. West, D. Cormier, *Int. J. Solids Struct.* **2015**, *69*, 475.
- [35] J. Dejun, L. Fanchun, Y. Zhang, *Sci. Rep.* **2020**, *10*, 600.
- [36] S. Liu, Y. Li, N. Li, *Mater. Des.* **2018**, *137*, 235.
- [37] O. Duncan, T. Allen, L. Foster, T. Senior, A. Alderson, *Acta Mater.* **2017**, *126*, 426.
- [38] F. Abd El-Sayed, R. Jones, I. Burgess, *Composites* **1979**, *10*, 209.
- [39] F. W. Zok, R. M. Latture, M. R. Begley, *J. Mech. Phys. Solids* **2016**, *96*, 184.
- [40] S. Ghuku, T. Mukhopadhyay, *Compos. Struct.* **2022**, <https://doi.org/10.1016/j.compstruct.2022.116318>.
- [41] P. Prajwal, S. Ghuku, T. Mukhopadhyay, *Mech. Mater.* **2022**, *171*, 104337.
- [42] S. Ghuku, T. Mukhopadhyay, *Int. J. Non-Linear Mech.* **2022**, *140*, 103887.
- [43] P. Sinha, T. Mukhopadhyay, *Thin-Walled Struct.* **2022**, *173*, 108950.
- [44] X. Zheng, H. Lee, T. H. Weisgraber, M. Shusteff, J. DeOtte, E. B. Duoss, J. D. Kuntz, M. M. Biener, Q. Ge, J. A. Jackson, S. O. Kucheyev, N. X. Fang, C. M. Spadaccini, *Science* **2014**, *344*, 1373.
- [45] M. P. Bendsøe, O. Sigmund, *Optimization of Structural Topology, Shape, and Material*, Vol. 414, Springer, Berlin **1995**.
- [46] M. P. Bendsoe, O. Sigmund, *Topology Optimization: Theory, Methods, and Applications*, Springer Science & Business Media, Berlin **2003**.
- [47] O. Sigmund, Ph.D. Thesis, *Technical University of Denmark*, Denmark **1994**.
- [48] J. López, N. Valizadeh, T. Rabczuk, *Comput. Methods Appl. Mech. Eng.* **2022**, *391*, 114564.
- [49] X. Huang, M. Xie, *Evolutionary Topology Optimization of Continuum Structures: Methods and Applications*, John Wiley & Sons, New York, NY **2010**.
- [50] H. A. Eschenauer, N. Olhoff, *Appl. Mech. Rev.* **2001**, *54*, 331.
- [51] P. Areias, H. Rodrigues, T. Rabczuk, *Eur. J. Mech. A Solids* **2021**, *85*, 104117.
- [52] T. E. Bruns, D. A. Tortorelli, *Comput. Methods Appl. Mech. Eng.* **2001**, *190*, 3443.
- [53] J.-H. Zhu, W.-H. Zhang, L. Xia, *Arch. Comput. Methods Eng.* **2016**, *23*, 595.
- [54] O. Sigmund, *Struct. Multidiscip. Optim.* **2001**, *21*, 120.
- [55] C. S. Andreasen, M. O. Elingaard, N. Aage, *Struct. Multidiscip. Optim.* **2020**, *62*, 685.
- [56] E. Andreassen, A. Clausen, M. Schevenels, B. S. Lazarov, O. Sigmund, *Struct. Multidiscip. Optim.* **2011**, *43*, 1.
- [57] S. Adhikari, T. Mukhopadhyay, X. Liu, *Mech. Mater.* **2021**, *157*, 103796.
- [58] X. Chen, Y. Liu, *Finite Element Modeling and Simulation with ANSYS Workbench*, CRC Press, Boca Raton FL **2018**.
- [59] A. Singh, T. Mukhopadhyay, S. Adhikari, B. Bhattacharya, *Compos. Struct.* **2022**, *280*, 114857.